

Saccorhytus is an early ecdysozoan and not the earliest deuterostome

<https://doi.org/10.1038/s41586-022-05107-z>

Received: 16 December 2021

Accepted: 13 July 2022

Published online: 17 August 2022

 Check for updates

Yunhuan Liu^{1,10}, Emily Carlisle^{2,10}, Huaqiao Zhang³✉, Ben Yang⁴, Michael Steiner^{5,6}, Tiequan Shao¹, Baichuan Duan⁷, Federica Marone⁸, Shuhai Xiao⁹✉ & Philip C. J. Donoghue²✉

The early history of deuterostomes, the group composed of the chordates, echinoderms and hemichordates¹, is still controversial, not least because of a paucity of stem representatives of these clades^{2–5}. The early Cambrian microscopic animal *Saccorhytus coronarius* was interpreted as an early deuterostome on the basis of purported pharyngeal openings, providing evidence for a meiofaunal ancestry⁶ and an explanation for the temporal mismatch between palaeontological and molecular clock timescales of animal evolution^{6–8}. Here we report new material of *S. coronarius*, which is reconstructed as a millimetric and ellipsoidal meiobenthic animal with spinose armour and a terminal mouth but no anus. Purported pharyngeal openings in support of the deuterostome hypothesis⁶ are shown to be taphonomic artefacts. Phylogenetic analyses indicate that *S. coronarius* belongs to total-group Ecdysozoa, expanding the morphological disparity and ecological diversity of early Cambrian ecdysozoans.

The microscopic animal *S. coronarius* was first reported from the early Cambrian⁹ (531.8–536.4 million years ago (Ma)) Kuanchuanpu Formation at the Zhangjiagou section in South China⁶. It was interpreted as an anusless, meiobenthic deuterostome⁶ largely on the basis of the presence of pharyngeal openings, one of the few deuterostome synapomorphies¹⁰. Thus, *S. coronarius* fills a critical gap in the deuterostome fossil record and represents an instance of loss of the anus in deuterostomes, which is known to have occurred several times independently in bilaterians¹¹. However, it has also been speculated that *S. coronarius* may be a stem scalidophoran or a primitive bilaterian¹². To test these phylogenetic interpretations and evolutionary implications of *S. coronarius*, we obtained new evidence on its morphology and ecology based on new material from the early Cambrian Kuanchuanpu Formation at the Zhangjiagou section^{13,14} (Figs. 1–3 and Extended Data Figs. 2–8) and Shizhonggou section¹⁵ (Extended Data Fig. 9) in Shaanxi Province, South China (see Extended Data Fig. 1 for localities). We characterized *S. coronarius* using both scanning electron microscopy (SEM) and synchrotron radiation X-ray tomographic microscopy¹⁶ (SRXTM), interpreted its morphology through a taphonomic lens, reconstructed its three-dimensional morphology and, on the basis of an expanded morphological database of metazoans, carried out a comprehensive phylogenetic analysis to establish its affinity^{6,12,13}.

Anatomy of *S. coronarius*

Most Zhangjiagou specimens are taphonomically flattened and subsequently abraded during transportation or sample preparation, but some are three-dimensionally preserved with a lesser extent of

deformation (Extended Data Fig. 2a,b and Supplementary Video 1). Only the exterior body wall is preserved; no internal organs are observed (Extended Data Figs. 2c and 3c,f). The body wall is composed of two layers and represents the preserved part of the integument (Figs. 1d and 2b and Extended Data Figs. 2d, 3c, 4a and 5e). No cilium insertion sites were observed on the integument, even in high-magnification SEM images. A chevron pattern is present in places on the integument (Fig. 3h and Extended Data Figs. 3h, 4e, 6f and 7a,c).

S. coronarius is ellipsoidal in overall shape, with a polar aperture that can be closed or open (Figs. 1a,f and 2f and Extended Data Figs. 2a,d, 3d, 4a,h, 5c, 6a,d, 7f and 8b). The aperture has various appearances depending on the degree of compression and closure, including as a flattened slit (Fig. 1b and Extended Data Figs. 7f and 8a), partially open with two V-shaped corners (Fig. 1f and Extended Data Figs. 2d, 3d, 4h, 5c and 6a) and, when fully open, approximately circular (Extended Data Figs. 6d and 8b). The closed polar aperture divides the body into two halves, with one half slightly wider than the other (Fig. 1a, Extended Data Fig. 2a,b and Supplementary Video 1).

The polar aperture is surrounded by radial folds of the integument (Figs. 1b,e,f and 2f and Extended Data Figs. 2d,f,g, 3d, 4a,c,h, 6a,d and 8a). The radial folds are internally pleated (Fig. 2g,h) and surrounded by a circlet of about 25–30 circumapertural protuberances that are in close contact with each other (Fig. 1f and Extended Data Figs. 2d and 4h). The circumapertural protuberances are internally hollow (Figs. 1b,e and 2f–h), largest at the midline, but decrease in size toward the sides (Fig. 1f and Extended Data Figs. 2d, 4h and 5c). Each of the circumapertural protuberances is flattened and tridentate, with a larger main spine flanked by two smaller lateral spines (Fig. 1g and Extended

¹School of Earth Science and Resources, Chang'an University, Xi'an, China. ²Bristol Palaeobiology Group, School of Earth Sciences, University of Bristol, Bristol, UK. ³State Key Laboratory of Palaeobiology and Stratigraphy, Nanjing Institute of Geology and Palaeontology and Center for Excellence in Life and Palaeoenvironment, Chinese Academy of Sciences, Nanjing, China. ⁴MNR Key Laboratory of Stratigraphy and Palaeontology, Institute of Geology, Chinese Academy of Geological Sciences, Beijing, China. ⁵College of Earth Science and Engineering, Shandong University of Science and Technology, Qingdao, China. ⁶Department of Earth Sciences, Freie Universität Berlin, Berlin, Germany. ⁷Key Laboratory of Marine Geology and Metallogeny, First Institute of Oceanography, Ministry of Natural Resource, Qingdao, China. ⁸Swiss Light Source, Paul Scherrer Institut, Villigen, Switzerland. ⁹Department of Geosciences, Virginia Tech, Blacksburg, VA, USA. ¹⁰These authors contributed equally: Yunhuan Liu, Emily Carlisle. ✉e-mail: hqzhang@nigpas.ac.cn; xiao@vt.edu; phil.donoghue@bristol.ac.uk

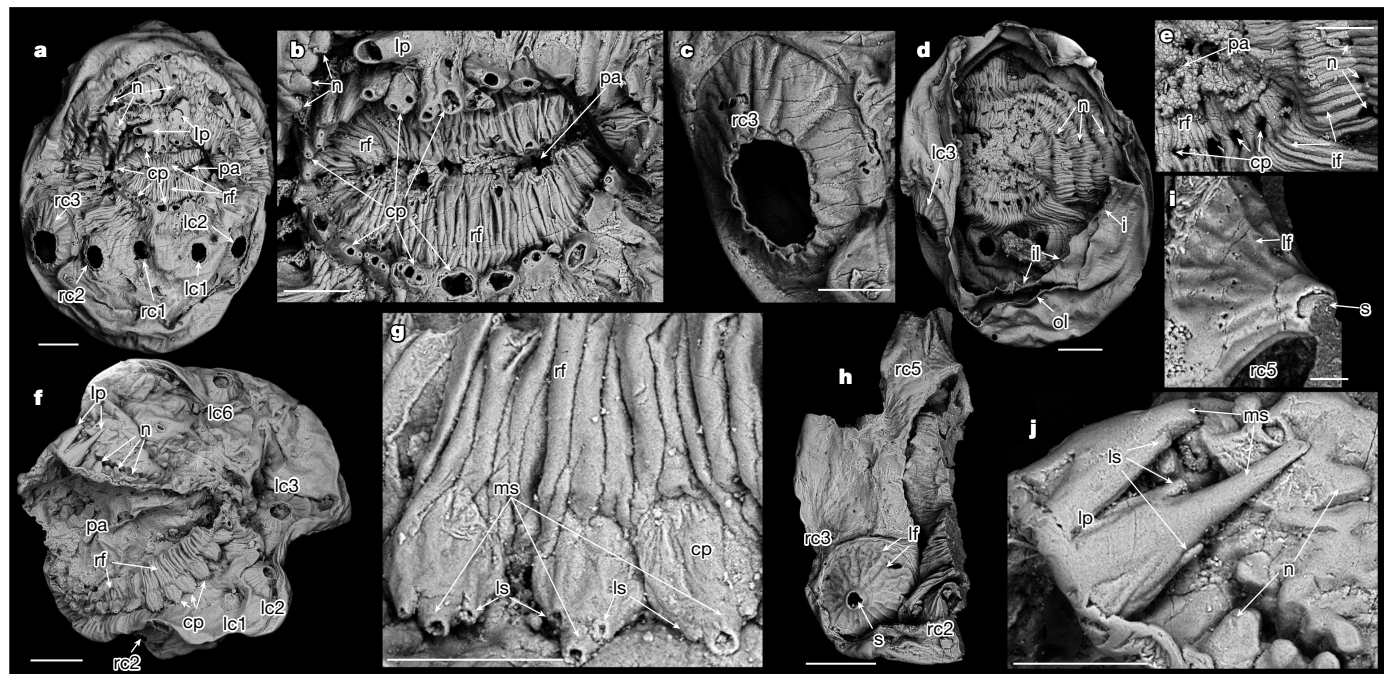


Fig. 1 | Anatomy of *S. coronarius*. **a–e**, UMCU2016009, with two large protuberances. **a**, Apertural view. **b**, Detail of polar aperture. **c**, Detail of broken third right body cone, with jagged edge exposing two integument layers. **d**, Opposite side of **a**, with abapertural integument missing, showing inner view of polar aperture and detached integument layers. **e**, Detail of inner side of aperture, showing hollow nature of circumapertural protuberances. **f, g, j**, UMCU2019016, with two large protuberances. **f**, Apertural lateral view. **g**, Detail of circumapertural protuberances. **j**, Detail of large protuberances. **h, i**, UMCU2018011. **h**, A fragment. **i**, Detail of fifth right body cone, showing

remnant of apical spine. **B**, base of body cone; **ch**, chevron; **cp**, circumapertural protuberance; **i**, integument; **if**, integument folds; **i/ol**, inner/outer integument layer; **lc**, left body cone (numbered assuming an anterior mouth and dorsal large protuberances); **lf**, longitudinal folds; **lp**, large protuberance; **ls**, lateral spine; **ms**, main spine; **n**, node; **pa**, polar aperture; **rc**, right body cone (numbered assuming an anterior mouth and dorsal large protuberances); **rf**, radial folds; **s**, apical spine of body cone; **sp**, small abapertural spine. Scale bars: 200 μm (**a, d, f, h**), 100 μm (**b, c, e, g, j**) and 20 μm (**i**).

Data Figs. 2f, g, 4g, 6c and 8e). In many specimens, the protuberances are broken at the base, leaving circular to rectangular openings on the integument (Figs. 1b and 2f). Abapertural of the circumapertural protuberances is an array of large protuberances that, unlike the circlet disposition of the circumapertural protuberances, are arranged in one or two rows on only one side of the polar aperture; when the aperture is flattened, the large protuberances are always arranged in line with, but never at the corners of, the flattened aperture. The number of large protuberances varies from one (Fig. 2a and Extended Data Figs. 3d and 5a), two (Figs. 1a, f and 2f and Extended Data Figs. 4a, h, 6a, d, 7f and 8b, c), three (Extended Data Fig. 2d), four (Extended Data Figs. 4c and 5c), to five (Extended Data Figs. 2a and 7d), possibly representing intraspecific or ontogenetic variation. They are arranged in one row if fewer than five, or in two rows if five. The large protuberances are also flattened and tridentate, with a main spine flanked by two lateral spines or denticles (Fig. 1j and Extended Data Figs. 4c, 6a and 8a, c, e). The circumapertural and large protuberances have similar morphology; the only difference is that the latter are larger and longer.

Further abapertural, there are numerous integument folds that are radially arranged (Fig. 1a, e and Extended Data Figs. 2d, 4a, c, 5c, 6a, d, 7b and 8b), as well as nodes or tubercles close to the large protuberances (Fig. 1a, f and Extended Data Figs. 2d, e, 4a, c, h, 5c, 6a, d and 7d). These nodes are arranged in crescent semi-circlets or sets parallel to disposition of the large protuberances. The first set of nodes are in line with the large protuberances and extend laterally (Fig. 1j and Extended Data Figs. 4a, c, 6a, d and 7d); the next two or three sets extend continuously to the sides, whereas the remaining two to three sets are more sparsely and less regularly arranged (Extended Data Figs. 4a, c and 7d), and further beyond are sometimes singularly disposed nodes (Extended Data Fig. 7d).

There are up to eight pairs of body cones around the body. Three pairs are arranged bilaterally in a row close to the side of the polar aperture opposite to the large protuberances (Figs. 1a, f, 2f and 3a and Extended Data Figs. 2d, 4a, i, 5c, d, 6d and 8b); of these, the medial pair (l/rc1) are the smallest, whereas the lateral-most pair (l/rc3) are the largest (Supplementary Table 1). Up to five additional pairs of body cones are found on the lateral and abapertural sides of the body. They are also arranged bilaterally (Fig. 3f, l and Extended Data Figs. 4b, j, 5c, d, 6e and 7b, e, g). The largest are the sixth pair (l/rc6; Supplementary Table 1), which are always present (Figs. 1f, 2a, c and 3b, f, j, l and Extended Data Figs. 2b, e, 3d, 4b, h, j, 5b, c, 6e, h, 7b, g and 8f), whereas the other body cones, particularly the seventh and eighth pairs (l/rc7 and l/rc8), may be absent (Fig. 1f and Extended Data Fig. 2e), probably reflecting intraspecific or ontogenetic variation.

Each body cone has an expanded conical base ornamented with longitudinal folds or ridges (Figs. 1c, h, i, 2a, b and 3c–e, h, k and Extended Data Figs. 3g, 4e, 5a, 6f, g and 8b). Completely preserved body cones have an apical spine with a closed tip (Figs. 2b, h, k and 3h, k and Extended Data Figs. 3i, 4k, 7a and 8d); however, most body cones are broken at the base or middle of the cone, at the junction between the conical base and the apical spine, or at the apical spine (Figs. 1c, h, i, 2a and 3c–e, j, l and Extended Data Figs. 2d, 4i, j, 7f and 8b). When preserved, apical spines are always adpressed on the body wall (thus protected from abrasion or breakage during fossil preparation), and they are about three to four times the height of the base in the fourth and fifth pairs of cones (Fig. 3h, k and Extended Data Figs. 3i and 4k), but can be proportionally shorter in the first to third and sixth pairs of cones (Figs. 2b and 3c–e). The first to third and sixth pairs of body cones are equivalent to the first to third and fourth pairs of body cones described by Han et al.⁶ SRXTM¹⁶ analysis shows that the conical bases have mineral preservation

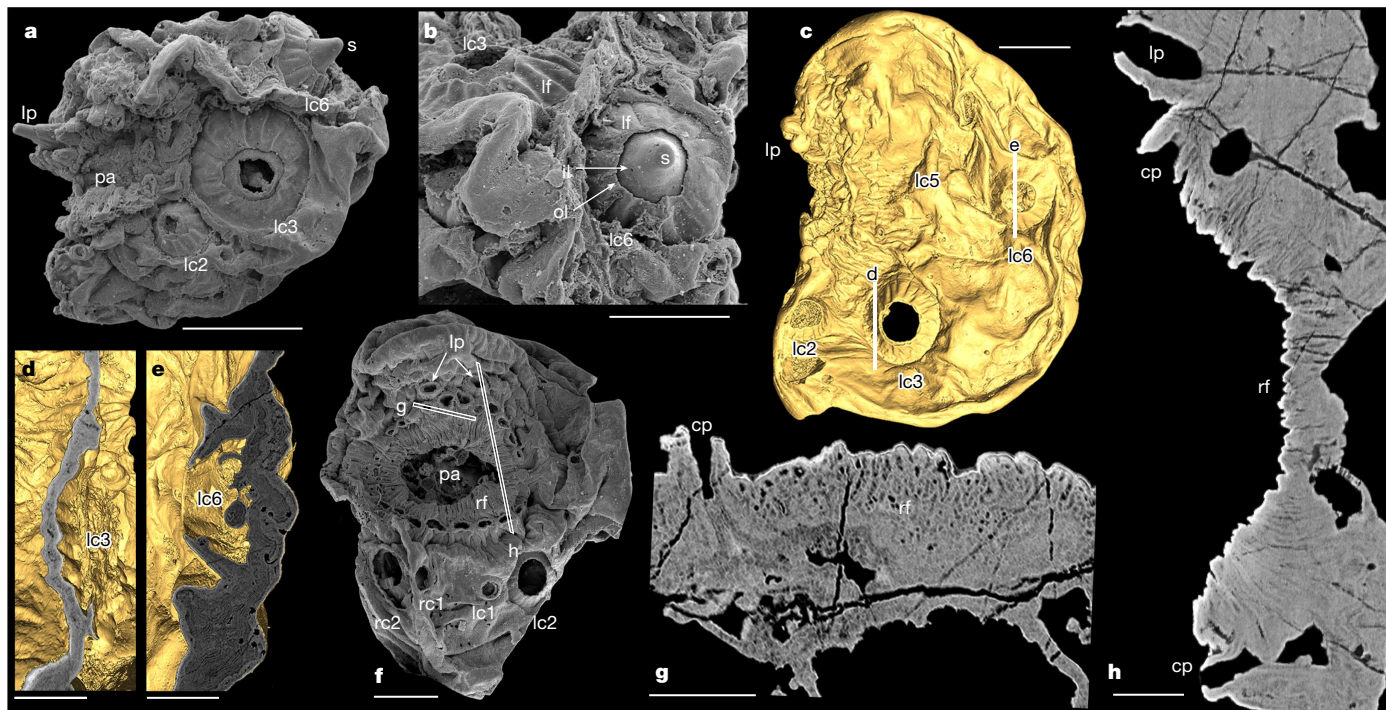


Fig. 2 | Anatomy of *S. coronarius*. **a, b**, He22-45, with a single large protuberance. **a**, Lateral view. **b**, Close-up view of sixth lateral body cone. **c–e**, He22-94, SRXTM images. **c**, Surface model, lateral view. **d, e**, Virtual sections through body cones as denoted in **c**. **f–h**, He22-57, with two large

protuberances. **f**, Apertural view. **g**, Virtual section through radial folds as denoted in **f**, bisecting a circumapertural protuberance. **h**, Virtual section through radial folds as denoted in **f**. Scale bars: 200 μm (**a, c, f**), 110 μm (**b**), 55 μm (**d**), 80 μm (**e**), 50 μm (**g, h**).

consistent with the surrounding integument but exhibit a distinct X-ray attenuation profile from the underlying layer (Fig. 2d,e).

On the abapertural side, there are numerous short and slender spines with a sharp tip that may extend beyond the eighth body cones (Fig. 3g,i and Extended Data Figs. 2e, 3h, 4b and 6e). The number and distribution of these spines are not uniform among different specimens. They may be randomly distributed and are basally separate from each other. They vary in size, with those around the eighth body cones slightly smaller than others, but they are generally much smaller than the body cones (Supplementary Table 1) and are typically broken from the base (Extended Data Figs. 4b, 5d and 6e). More completely preserved spines tend to be addressed against the integument (Fig. 3g,i) and thus were not abraded during fossil preservation or preparation.

Shizhonggou specimens (Extended Data Figs. 1b and 9) are similar to the Zhangjiagou specimens described above and in Han et al.⁶. They share key structures such as a polar aperture surrounded by radial folds (Extended Data Fig. 9e), two-layered integument (Extended Data Fig. 9b,d), body cones with a conical base and an apical spine (Extended Data Fig. 9a,c,e), and small abapertural spines (Extended Data Fig. 9a,c,f). These structures identify the Shizhonggou specimens as *Saccorhytus*.

Taphonomy and preservation

Although no internal anatomy is preserved in the Zhangjiagou and Shizhonggou specimens, microstructures in the two-layered integument inform us about fossilization processes and aid in biological and taphonomic interpretations. The two integument layers can be separated from each other by a gap (Fig. 1d) or tightly addressed to each other with no gaps in between, as observed by both SEM (Extended Data Fig. 5e) and SRXTM¹⁶ (Extended Data Fig. 3c). The tightly addressed layers cannot be phosphatic coatings on both sides of a substrate that has since been lost, in which case a gap would be present between the layers. Rather, they probably represent two integumentary layers that

were secondarily phosphatized through mineral impregnation. The mineralization may have occurred before and after the taphonomic detachment of the two layers, resulting in both addressed and separated integument layers. This interpretation is consistent with random orientation of the nanometre-scale apatite crystals that replicate the integument layer (Extended Data Fig. 5f), because phosphatic impregnation tends to be accomplished by randomly oriented nanocrystals whereas phosphatic encrustation results in apatite crystals that orient perpendicular to and grow away from the substrate¹⁷.

SRXTM analysis¹⁶ shows that the outer integument layer has a lower X-ray attenuation profile and preserves surface wrinkles and spines across the body surface; the inner integument layer exhibits a higher attenuation profile and is associated with, but not limited to, centripetal void-filling mineralization (Extended Data Fig. 9b). In places, the inner layer is detached from the outer layer (Extended Data Fig. 9d). The detached layers preserve complementary symmetry (Extended Data Fig. 9d) and can be virtually re-attached to restore their original configuration. There is no brittle deformation associated with this localized layer separation (Fig. 1d), indicating that it occurred prior to mineralization, associated with decay, with the inner layer delaminating from the outer and collapsing inward. In some of the compressed specimens, instead of two clear layers there is a thick layer of homogeneous mineralization around the entire body, surrounded by centrifugal and centripetal infilling visible as concentric layers (Fig. 2e). The homogeneous layer is continuous with the radial folds and protuberances located around the polar aperture (Fig. 2g,h) as well as with the body cones, indicating that this mineral phase preserves original biological structure. In other specimens, there are few visible layers of mineralization, with most of the interior of the specimen displaying the same high X-ray attenuation profile (Extended Data Fig. 2c), but the key anatomical features are still present on the surface, indicating that they are endocasts of the surface integument layer which is either not preserved or has been lost after preservation.

The symmetry of *S. coronarius* is anchored on the polar aperture. This aperture is the only body opening and is here interpreted as the mouth,

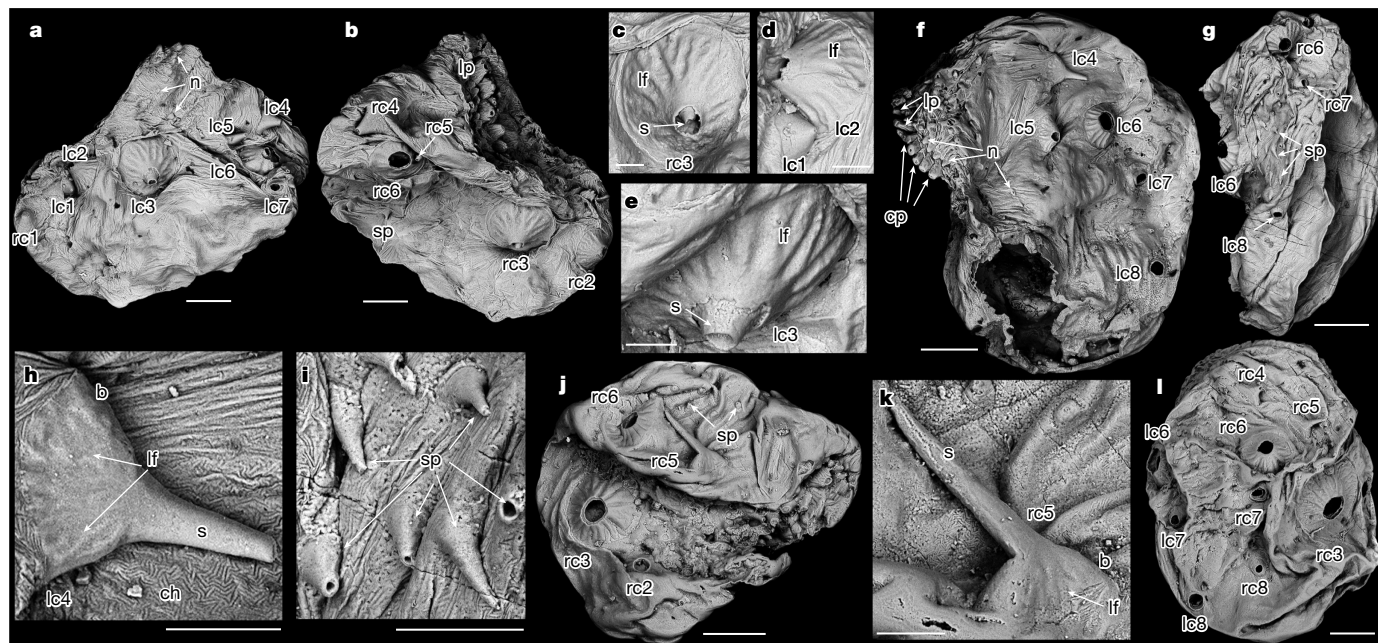


Fig. 3 | Anatomy of *S. coronarius*. **a–e**, UMCU2020021. **a**, Lateral view. **b**, Right view. **c–e**, Detail of body cones tilted approximately 40° from **a, b**, showing remnant of apical spine. **f, h**, UMCU2016008. **f**, Lateral view. **h**, Detail of fourth lateral body cone addressed against body wall. **g, i**, UMCU2016010.

g, Abapertural view. **i**, Detail of small abapertural spines addressed against body wall. **j, k**, UMCU2018012. **j**, Right view. **k**, Detail of fifth right body cone addressed against body wall. **l**, UMCU2019018, abapertural lateral view. Scale bars: 200 μ m (**a, b, f, g, j, l**), 60 μ m (**c–e, h, i, k**).

with the radial folds controlling its opening and closure, whereas a distinct anus is absent. The terminal mouth defines an oral–aboral body axis, the symmetrical arrangement of the body cones imparts the animal with a bilateral symmetry (that is, left and right sides), and the polarized distribution of large protuberances and nodes indicate the existence of a third body axis that is orthogonal to the oral–aboral and left–right axes. *Saccorhytus* thus has three main body axes. Guided by extant animals with three body axes—that is, the bilaterians¹⁸—we identify the three main body axes in *Saccorhytus* as being homologous to the anterior–posterior, dorsoventral and left–right axes of bilaterians. Therefore, *Saccorhytus* is reconstructed as a sac-like bilaterian with spinose armour and a terminal mouth but no anus (Fig. 4a–c and Supplementary Video 2); this reconstruction is different from that of Han et al.⁶, who placed the mouth ventrally.

The bilateral symmetry with anterior–posterior, dorsoventral and left–right axes suggests that *Saccorhytus* is phylogenetically affiliated with the Bilateria¹⁸. *Saccorhytus* lacks an anus, but this condition may represent either primitive or secondary absence (loss), considering that a through gut with a terminal anus may have evolved independently in different bilaterian lineages¹⁹ and loss of the anus has also occurred several times independently in different bilaterian groups¹¹. The previously proposed deuterostome hypothesis⁶ was based on similarities between the body cones of *Saccorhytus* and the body openings (interpreted as pharyngeal openings) of vetulicolians²⁰ and vetulocystids²¹. Better preserved specimens illustrated here (Figs. 1h, 2b and 3c, e, h, k and Extended Data Figs. 3i, 4k and 9e), however, show that the body cones in *Saccorhytus* have a closed apical spine and they are probably stiffened sclerites. *Saccorhytus* thus lacks homologues of pharyngeal openings¹⁸ and, as such, cannot be considered as a deuterostome.

Phylogenetic analysis and affinity

To resolve the phylogenetic affinity and evolutionary significance of *Saccorhytus*, we assembled a dataset of phenotypic characters from the diversity of metazoan phyla^{22–26}, which was subjected to Bayesian phylogenetic analysis in MrBayes²⁷. Our dataset recovers monophyletic

Bilateria, Protostomia, Ecdysozoa, Deuterostomia and Coelenterata, with a partial constraint to resolve Lophotrochozoa (Extended Data Fig. 10a). Within this framework, *Saccorhytus* is resolved as a total-group ecdysozoan (Extended Data Fig. 10a).

To account for the uncertainties about the phylogenetic affinity of the Xenacoelomorpha (as a deuterostome or a basal bilaterian²⁸), the monophyly of the Deuterostomia²⁹, and the monophyly of the Coelenterata^{22,30,31}, we conducted additional analyses with partial topology constraints (Supplementary Information, ‘Phylogenetic analyses’). In these analyses, *Saccorhytus* was consistently resolved as part of a polytomy at the base of total-group Ecdysozoa (Extended Data Fig. 10b, c). The topology of the phylogenetic results (Extended Data Fig. 10) indicates that *Saccorhytus* could be a basal ecdysozoan, a basal panarthropodan or a basal cycloneuralian (Fig. 4d).

To test the robustness of the total-group ecdysozoan interpretation, we carried out stepping-stone analyses to compare the Bayes factors of trees where *Saccorhytus* is constrained to Ecdysozoa, Deuterostomia⁶ or Coelenterata (a position that appeared in a small number of suggested trees from our Bayesian analyses). The model in which *Saccorhytus* is constrained to Ecdysozoa has overwhelmingly positive support compared with Deuterostomia (ln(Bayes factor) of 11.915, with $2\ln B_{12}$ of 23.83) and Coelenterata (ln(Bayes factor) of 5.54, with $2\ln B_{12}$ of 11.08) models³² (where B_{12} is the Bayes factor). We can therefore confidently rule out a deuterostome or coelenterate affinity for *Saccorhytus*. The ecdysozoan interpretation is consistent with the observation that most specimens are deflated, deformed and preserved with integuments but no internal anatomy, indicating that they may be cuticles or cuticular exuviae that are more decay-resistant than the soft internal tissues³³. This interpretation is different from that of Han et al.⁶, who coded the integumental layer as an epidermis in their character matrix.

Conclusions

The small body size of *Saccorhytus* indicates a meiobenthic lifestyle. The non-ciliated integument implies that it did not have cilia for locomotion or feeding. *Saccorhytus* also lacked setae or paired appendages,

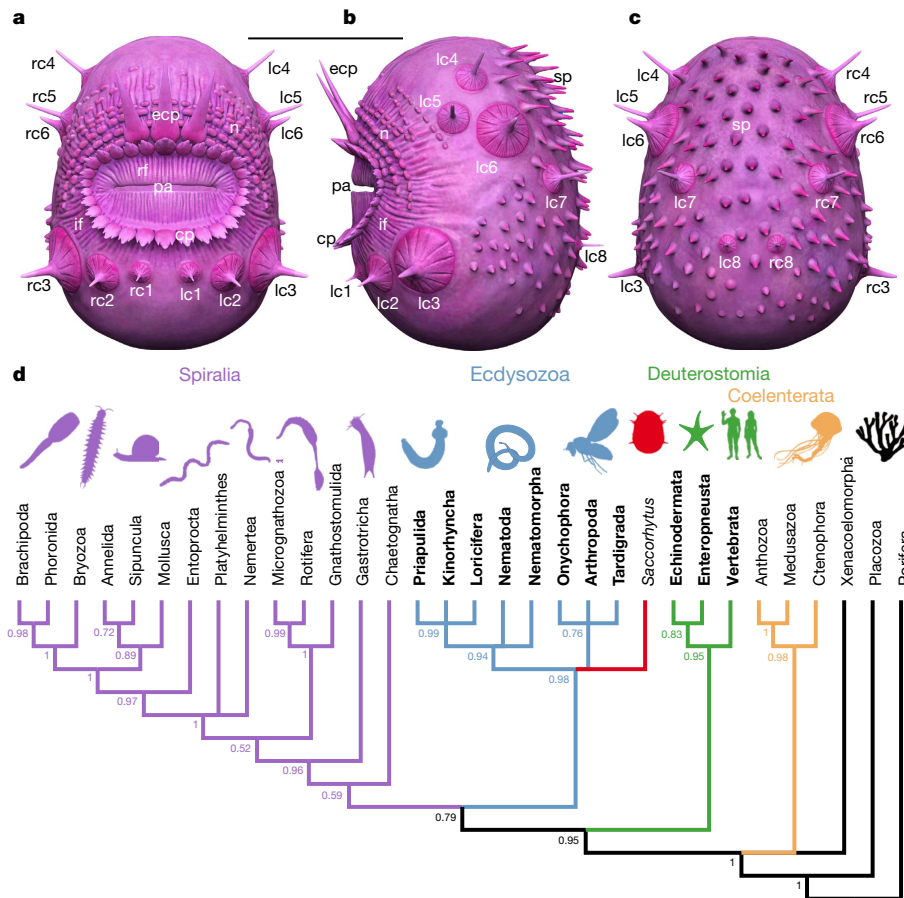


Fig. 4 | Reconstruction and phylogenetic interpretation of *S. coronarius*. **a–c**, Reconstructions showing anterior or apertural (**a**), left (**b**), and posterior or abapertural (**c**) views. Scale bar, 500 μ m. **d**, Phylogeny of Metazoa based on Extended Data Fig. 10, and possible position of *Saccorhytus*, based on Bayesian

phylogenetic analysis of a phenotypic dataset using the Mk model implemented in MrBayes 3.2.7a²⁷ (see Supplementary Information, 'Phylogenetic analyses'). Animal icons from phylopic.org.

and was thus unable to creep or crawl. Locomotion by hydrostatic skeleton is possible if its integument was flexible. *Saccorhytus* was probably a free epibenthic or interstitial meiofaunal animal living in a low-Reynolds-number environment. It is also possible that muscles may have been attached to its body cones that may have provided leverage for locomotion. Whereas the two-layered integument may represent cuticular structures with two sub-layers, the circumapertural protuberances, large protuberances, body cones and small abapertural spines are probably sclerotized cuticular structures and may have functioned as sensory and/or defence structures, whereas the mouth is the only body opening that must have functioned for feeding and excretion.

To summarize, *Saccorhytus* does not have pharyngeal openings and is not a deuterostome. It is instead a total-group ecdysozoan (Fig. 4d). Together with co-occurring cycloneuralians from the Zhangjiagou section^{34–36} and equivalent strata in South China^{37,38}, *Saccorhytus* testifies to the remarkable morphological disparity and ecological diversity of early Cambrian ecdysozoans and presents another case of secondary absence of the anus in ecdysozoans¹¹.

Online content

Any methods, additional references, Nature Research reporting summaries, source data, extended data, supplementary information, acknowledgements, peer review information; details of author contributions and competing interests; and statements of data and code availability are available at <https://doi.org/10.1038/s41586-022-05107-z>.

- Peterson, K. J. & Eernisse, D. J. The phylogeny, evolutionary developmental biology, and paleobiology of the Deuterostomia: 25 years of new techniques, new discoveries, and new ideas. *Org. Divers. Evol.* **16**, 401–418 (2016).
- Gee, H. On being vetulicolian. *Nature* **414**, 407–408 (2001).
- Aldridge, R. J., Hou, X., Siveter, D. J., Siveter, D. J. & Gabbott, S. E. The systematics and phylogenetic relationships of vetulicolians. *Palaeontology* **50**, 131–168 (2007).
- Topper, T. P., Guo, J., Clausen, S., Skovsted, C. & Zhang, Z. A stem group echinoderm from the basal Cambrian of China and the origins of Ambulacraria. *Nat. Commun.* **10**, 1366 (2019).
- Zamora, S. et al. Re-evaluating the phylogenetic position of the enigmatic early Cambrian deuterostome *Yanjiahella*. *Nat. Commun.* **11**, 1286 (2020).
- Han, J., Conway Morris, S., Ou, Q., Shu, D. & Huang, H. Meiofaunal deuterostomes from the basal Cambrian of Shaanxi (China). *Nature* **542**, 228–231 (2017).
- Rahman, I. A. Tiny fossils in the animal family tree. *Nature* **542**, 170–171 (2017).
- Gee, H. A (Very) Short History of Life on Earth: 4.6 Billion Years in 12 Pithy Chapters (Pan Macmillan, 2021).
- Peng, S., Babcock, L. E. & Ahlberg, P. in *Geological Time Scale 2020* (eds Gradstein, F. M. et al.) 565–629 (Elsevier, 2020).
- Lowe, C. J., Clarke, D. N., Medeiros, D. M., Rokhsar, D. S. & Gerhart, J. The deuterostome context of chordate origins. *Nature* **520**, 456–465 (2015).
- Hejnol, A. & Martín-Durán, J. M. Getting to the bottom of anal evolution. *Zool. Anz.* **256**, 61–74 (2015).
- Shu, D. & Han, J. The core value of Chengjiang fauna: the formation of the animal kingdom and the birth of basic human organs. *Earth Sci. Front.* **27**, 382–412 (2020).
- Liu, Y., Zhang, H., Xiao, S., Shao, T. & Duan, B. An early Cambrian ecdysozoan with a terminal mouth but no anus. Preprint at *bioRxiv* <https://doi.org/10.1101/2020.09.04.283960> (2020).
- Shao, T. et al. Diversity of cnidarians and cycloneuralians in the Fortunian (early Cambrian) Kuanchuanpu Formation at Zhangjiagou, South China. *J. Paleontol.* **92**, 115–129 (2018).
- Steiner, M., Li, G., Qian, Y. & Zhu, M. Lower Cambrian small shelly fossils of northern Sichuan and southern Shaanxi (China), and their biostratigraphic importance. *Geobios* **37**, 259–275 (2004).
- Donoghue, P. C. J. et al. Synchrotron X-ray tomographic microscopy of fossil embryos. *Nature* **442**, 680–683 (2006).
- Xiao, S. & Schiffbauer, J. D. in *From Fossils to Astrobiology* (eds Seckbach, J. & Walsh, M.) 89–117 (Springer-Verlag, 2009).

18. Nielsen, C. *Animal Evolution: Interrelationships of the Living Phyla* (Oxford Univ. Press, 2012).
19. Hejnol, A. & Martindale, M. Q. Acoel development indicates the independent evolution of the bilaterian mouth and anus. *Nature* **456**, 382–386 (2008).
20. Shu, D. et al. Primitive deuterostomes from the Chengjiang Lagerstätte (Lower Cambrian, China). *Nature* **414**, 419–424 (2001).
21. Shu, D., Conway Morris, S., Han, J., Zhang, Z. & Liu, J. Ancestral echinoderms from the Chengjiang deposits of China. *Nature* **430**, 422–428 (2004).
22. Zhao, Y. et al. Cambrian sessile, suspension feeding stem-group ctenophores and evolution of the comb jelly body plan. *Curr. Biol.* **29**, 1112–1125 (2019).
23. Sun, H. et al. Hyoliths with pedicles illuminate the origin of the brachiopod body plan. *Proc. R. Soc. B* **285**, 7 (2018).
24. Vinther, J. & Parry, L. A. Bilateral jaw elements in *Amiskwia sagittiformis* bridge the morphological gap between gnathiferans and chaetognaths. *Curr. Biol.* **29**, 881–888 (2019).
25. Bekkouche, N. & Worsaae, K. Nervous system and ciliary structures of Micrognathozoa (Gnathifera): evolutionary insight from an early branch in Spiralia. *R. Soc. Open Sci.* **3**, 17 (2016).
26. Hejnol, A. & Lowe, C. J. Embracing the comparative approach: how robust phylogenies and broader developmental sampling impacts the understanding of nervous system evolution. *Phil. Trans. R. Soc. B* **370**, 16 (2015).
27. Ronquist, F. et al. MrBayes 3.2: efficient Bayesian phylogenetic inference and model choice across a large model space. *Syst. Biol.* **61**, 539–542 (2012).
28. Kapli, P. & Telford, M. J. Topology-dependent asymmetry in systematic errors affects phylogenetic placement of Ctenophora and Xenacoelomorpha. *Sci. Adv.* **6**, 11 (2020).
29. Kapli, P. et al. Lack of support for Deuterostomia prompts reinterpretation of the first Bilateria. *Sci. Adv.* **7**, eabe2741 (2021).
30. Peterson, K. J. & Eernisse, D. J. Animal phylogeny and the ancestry of bilaterians: inferences from morphology and 18S rDNA gene sequences. *Evol. Dev.* **3**, 170–205 (2001).
31. Philippe, H. et al. Phylogenomics revives traditional views on deep animal relationships. *Curr. Biol.* **19**, 706–712 (2009).
32. Nylander, J. A. A., Ronquist, F., Huelsenbeck, J. P. & Nieves-Aldrey, J. L. Bayesian phylogenetic analysis of combined data. *Syst. Biol.* **53**, 47–67 (2004).
33. Gostling, N. J., Dong, X.-P. & Donoghue, P. C. J. Ontogeny and taphonomy: An experimental taphonomy study of the development of the brine shrimp *Artemia salina*. *Palaeontology* **52**, 169–186 (2009).
34. Liu, Y., Xiao, S., Shao, T., Broce, J. & Zhang, H. The oldest known priapulid-like scalidophoran animal and its implications for the early evolution of cycloneuralians and ecdysozoans. *Evol. Dev.* **16**, 155–165 (2014).
35. Liu, Y. et al. New armoured scalidophorans (Ecdysozoa, Cycloneuralia) from the Cambrian Fortunian Zhangjiagou Lagerstätte, South China. *Pap. Palaeontol.* **5**, 241–260 (2019).
36. Shao, T. et al. New macrobenthic cycloneuralians from the Fortunian (lowermost Cambrian) of South China. *Precambrian Res.* **349**, 105413 (2020).
37. Zhang, H. et al. Armored kinorhynch-like scalidophoran animals from the early Cambrian. *Sci Rep.* **5**, 16521 (2015).
38. Zhang, H., Maas, A. & Waloszek, D. New material of scalidophoran worms in Orsten-type preservation from the Cambrian Fortunian Stage of South China. *J. Paleontol.* **92**, 14–25 (2018).

Publisher's note Springer Nature remains neutral with regard to jurisdictional claims in published maps and institutional affiliations.

Springer Nature or its licensor holds exclusive rights to this article under a publishing agreement with the author(s) or other rightsholder(s); author self-archiving of the accepted manuscript version of this article is solely governed by the terms of such publishing agreement and applicable law.

© The Author(s), under exclusive licence to Springer Nature Limited 2022

Methods

The fossil specimens were recovered from the early Cambrian Kuan-chuanpu Formation at Zhangjiagou section¹⁴ (specimen numbers with prefix UMCU or He) and Shizhonggou section¹⁵ (specimen numbers with prefix KYuan), China (Extended Data Fig. 1). The key horizons at both sections yielding *Saccorhytus* specimens fall within the small shelly fossil *Anabarites trisulcatus-Protohertzina anabarica* Assemblage Zone^{14,39,40} and have a time span⁹ of 531.8–536.4 Ma, belonging to the Cambrian Fortunian stage. Rock samples from these two sections were macerated using diluted acetic acid (10%), and microfossils were handpicked from residues under a binocular microscope. The University Museum of Chang'an University (UMCU) specimens were glued on pin-type aluminium stubs with diluted milk glue for observation under a LEO 1530VP field-emission environmental scanning electron microscope, a Hitachi SU3500 scanning electron microscope, and a field-emission scanning electron microscope TESCAN MAIA3 at the Nanjing Institute of Geology and Palaeontology, Chinese Academy of Sciences. The Freie Universität Berlin (FUB) specimens were rinsed in pure ethanol, mounted on aluminium sample stubs with adhesive carbon film and sputtered for 6 min with gold in a BioRad elemental SEM coating system, and then observed under a ZEISS Supra 40 VP Ultra at the Department of Earth Sciences, Freie Universität Berlin.

SRXTM¹⁶ was conducted at the X02DA TOMCAT beamline of the Swiss Light Source, Paul Scherrer Institut, Villigen, Switzerland. Projections were obtained with beam energies of 15–22.5 KeV, exposures of 150–860 ms, using a 20 µm LuAg:Ce scintillator, 10× and 20× objectives, yielding reconstructed tomographic data with voxel dimensions of 0.65 µm and 0.325 µm, respectively. A total of 1,501 projections were taken equi-angularly through 180° rotation within the beam. Projections were post-processed and rearranged into flat- and dark-field-corrected sinograms, and reconstruction was performed on a 60-core Linux PC farm, using a highly optimized routine based on the Fourier transform method and a regridding procedure⁴¹. Slice data were analysed and manipulated using VGStudioMax (www.volumegraphics.com) and AVIZO (www.thermofisher.com/avizo/software).

Phylogenetic analyses were conducted based on our updated description and reconstruction of *S. coronarius*, a broad sampling of animal taxa, and a comprehensive coding of 134 morphological characters. The data matrix was subjected to Bayesian phylogenetic analysis under the Mk model⁴² implemented in MrBayes 3.2²⁷.

Inclusion and ethics

The research described in this study included local researchers from the initial stages of design through execution, analysis, interpretation and publication. All researchers who contributed to the study are recognized through authorship. We were provided with permission for sampling through formal agreements with the Nanjing Institute of Geology and Palaeontology (NIGPAS), Chinese Academy of Sciences, extending back to 2000.

Reporting summary

Further information on research design is available in the Nature Research Reporting Summary linked to this article.

Data availability

The data that support the findings of this study are available in the paper and its Supplementary Information, or from the corresponding authors upon reasonable request. All specimens illustrated in this paper are deposited at the University Museum of Chang'an University (accession numbers UMCU2014001–2014005, 2016006–2016010, 2018011–2018015, 2019016–2019020 and 2020021–2020025), and at the Department of Earth Sciences, Freie Universität Berlin (accession numbers He22-45, He22-57, He22-94, KYuan26, KYuan55 and KYuan102). Tomographic data are freely available from the University of Bristol data repository, data.bris, at https://doi.org/10.5523/bris.2iha22zob_eher2leh936xrktqx.

Code availability

The phylogenetic dataset, commands, and topological constraints necessary to run the MrBayes analyses are included as NEXUS formatted files in the Supplementary Information.

- Steiner, M., Qian, Y., Li, G., Hagadorn, J. W. & Zhu, M. The developmental cycles of early Cambrian Olivoidae fam. nov. (?Cycloneuralia) from the Yangtze Platform (China). *Palaeogeogr. Palaeoclimatol. Palaeoecol.* **398**, 97–124 (2014).
- Steiner, M., Li, G., Qian, Y., Zhu, M. & Erdtmann, B.-D. Neoproterozoic to early Cambrian small shelly fossil assemblages and a revised biostratigraphic correlation of the Yangtze Platform (China). *Palaeogeogr. Palaeoclimatol. Palaeoecol.* **254**, 67–99 (2007).
- Marone, F., Studer, A., Billich, H., Sala, L. & Stamparoni, M. Towards on-the-fly data post-processing for real-time tomographic imaging at TOMCAT. *Adv. Structural Chem. Imaging* **3**, 1 (2017).
- Lewis, P. O. A likelihood approach to estimating phylogeny from discrete morphological character data. *Syst. Biol.* **50**, 913–925 (2001).

Acknowledgements This work was supported by National Natural Science Foundation of China (nos. 41872014, 42172020 and 41972026, Research Fund for International Senior Scientists 2021), Strategic Priority Research Program of Chinese Academy of Sciences (no. XDB26000000), State Key Laboratory of Palaeobiology and Stratigraphy, Nanjing Institute of Geology and Palaeontology, Chinese Academy of Sciences (no. 20191104). E.C. was supported by a University of Bristol Scholarship; M.S. was funded by Deutsche Forschungsgesellschaft (STE814/5-1); S.X. was supported by the U.S. National Science Foundation (EAR-2021207); P.C.J.D. was funded by Natural Environment Research Council (NERC) grant (NE/P013678/1), part of the Biosphere Evolution, Transitions and Resilience (BETR) programme, which is co-funded by the Natural Science Foundation of China (NSFC), as well as the Leverhulme Trust (RF-2022-167). We acknowledge the Paul Scherrer Institut, Villigen, Switzerland for provision of synchrotron radiation beamtime at the TOMCAT beamline of the SLS. We thank D. Yang for assistance with artistic reconstructions and F. Dunn for data that contributed to our phylogenetic analyses.

Author contributions H.Z. and P.C.J.D. designed the research. Y.L., T.S., B.Y. and M.S. obtained the fossils. H.Z. and M.S. carried out SEM work. E.C., F.M. and P.C.J.D. collected SRXTM data. E.C. and B.D. analysed SRXTM data. E.C. and P.C.J.D. conducted phylogenetic analyses. H.Z., E.C., S.X., M.S. and P.C.J.D. developed the interpretation. H.Z. wrote the first draft of the manuscript, with contributions from all other authors.

Competing interests The authors declare no competing interests.

Additional information

Supplementary information The online version contains supplementary material available at <https://doi.org/10.1038/s41586-022-05107-z>.

Correspondence and requests for materials should be addressed to Huaqiao Zhang, Shuhai Xiao or Philip C. J. Donoghue.

Peer review information Nature thanks the anonymous reviewers for their contribution to the peer review of this work.

Reprints and permissions information is available at <http://www.nature.com/reprints>.